Supporting Information

Carbon hollow tube confined Sb/Sb_2S_3 nanorod fragments as a highly stable anode for potassium ion batteries

Yuanji Wu[a], Jiefeng Zheng[a], Yong Tong[a], Xi Liu[a], Yingjuan Sun[a]*, Li Niu[b] and Hongyan Li[a]*

[a] *Department of Materials Science and Engineering, College of Chemistry and Materials Science, Jinan University, Guangzhou 510632, China*

[b] *Center for Advanced Analytical Science, Guangzhou University, Guangzhou 510006, China*

*E-mail: lihongyan@jnu.edu.cn and yjsun@jnu.edu.cn

Contents list

Ⅰ. Supplementary Results and Discussion

Ⅱ. Reference

Ⅰ. Supplementary Results and Discussion

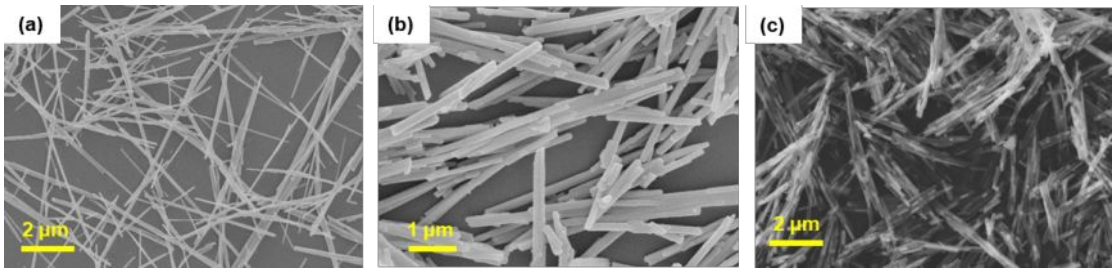

Figure S1. SEM images of Sb_2S_3 nanorods (a), Sb_2S_3@PDA (b), Sb/Sb_2S_3@CHT (c), respectively.

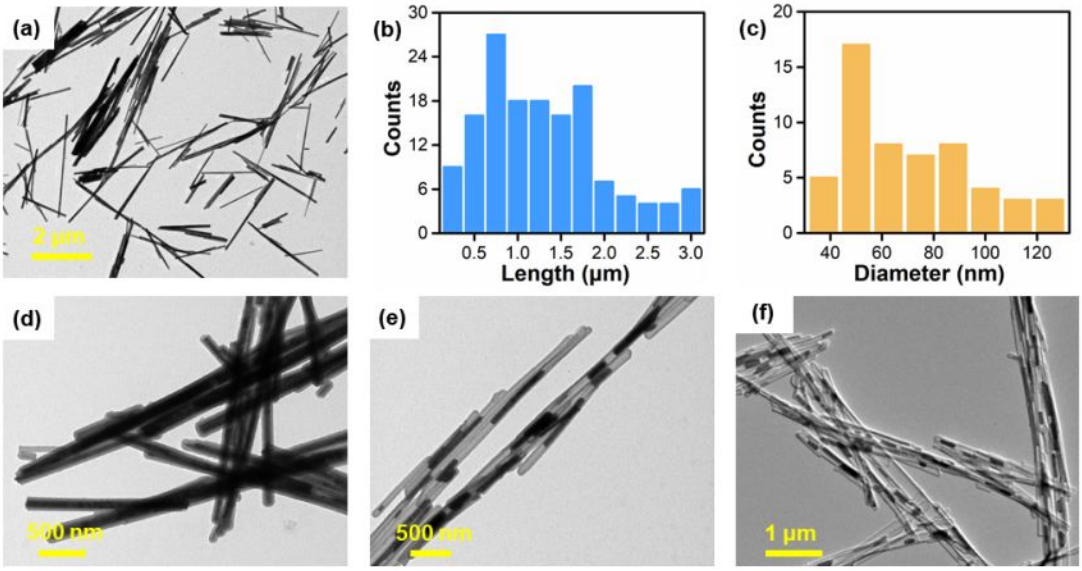

Figure S2. (a) TEM image of Sb_2S_3 nanorods. (b-c) Statistical distribution diagram of the length and diameter of Sb_2S_3 nanorods. (d) TEM image of Sb_2S_3@PDA. (e-f) TEM images of Sb/Sb_2S_3@CHT.

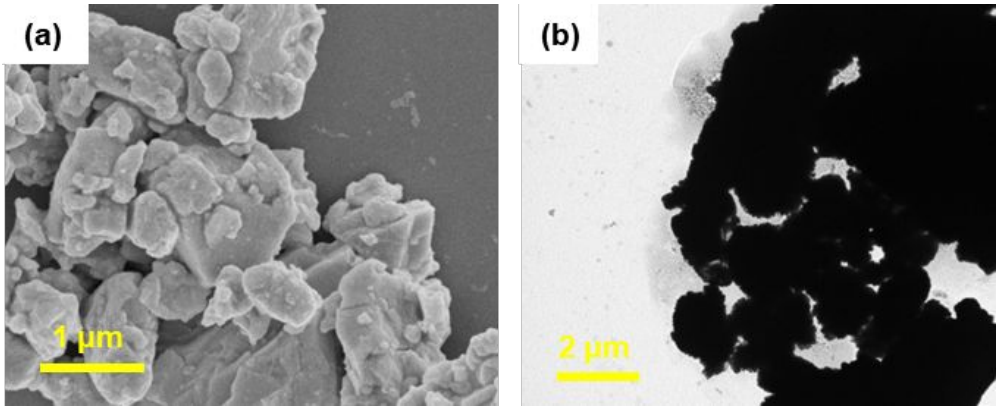

Figure S3. SEM (a) and TEM (b) images of commercial Sb powders.

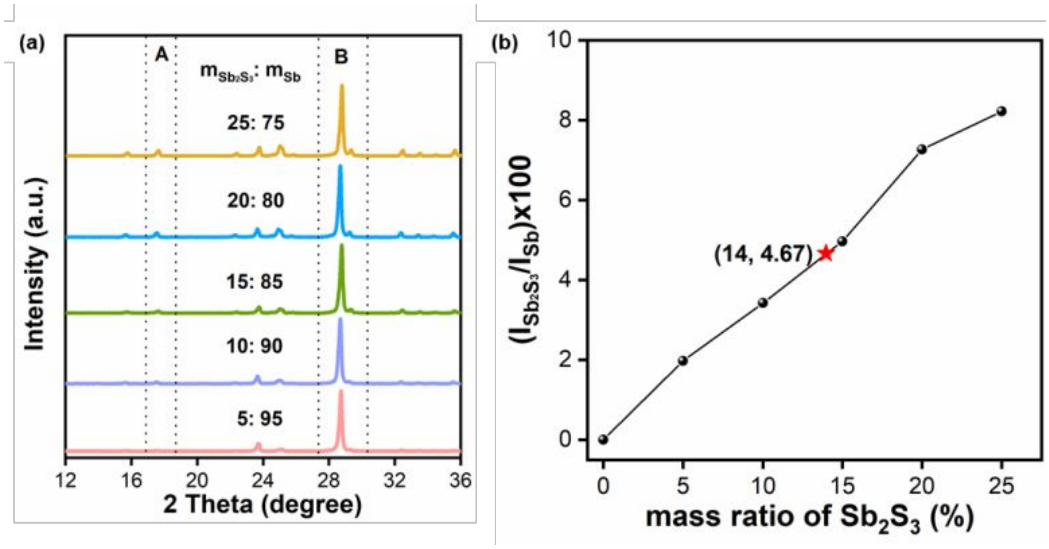

Figure S4. (a)XRD patterns of Sb/Sb_2S_3 hybrids with different mass ratios. (b) The relationship between I_{Sb2S3}/I_{Sb} and the mass ratio of Sb_2S_3 in Sb/Sb_2S_3 hybrid. The I_{Sb2S3}/I_{Sb} is calculated by $I_A/(I_B-I_A/0.8586)$. In pure Sb_2S_3 pattern, $I_A/I_B=0.8586$. The star symbol is the value estimated by the XRD pattern of Sb/Sb_2S_3@C.

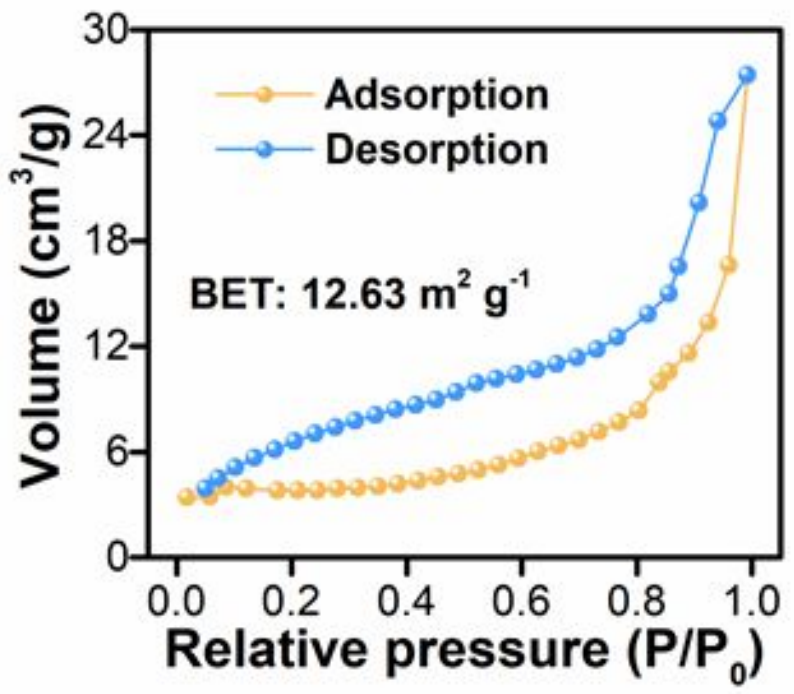

Figure S5. N_2 adsorption-desorption isotherm curve of Sb/Sb_2S_3@CHT.

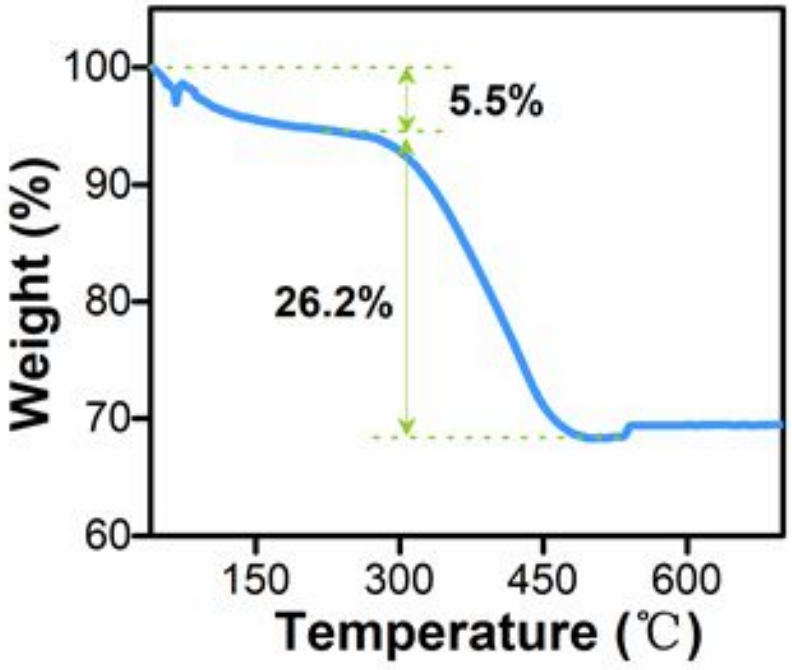

Figure S6. Thermogravimetric curve of Sb/Sb_2S_3@CHT.

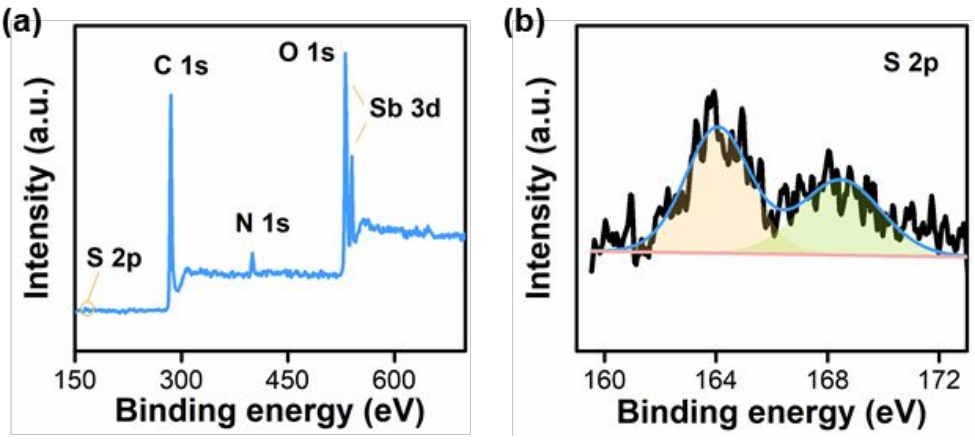

Figure S7. (a) XPS survey spectrum and (b) High-resolution S 2p spectrum of Sb/Sb_2S_3@CHT.

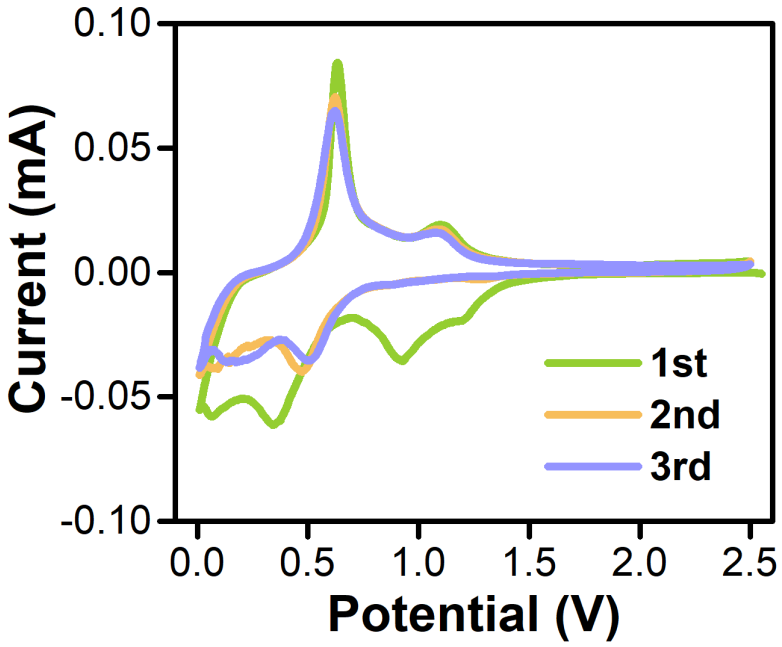

Figure S8. The first three CV curves of Sb_2S_3 anode with a scanning rate of 0.05 mV s^{-1}.

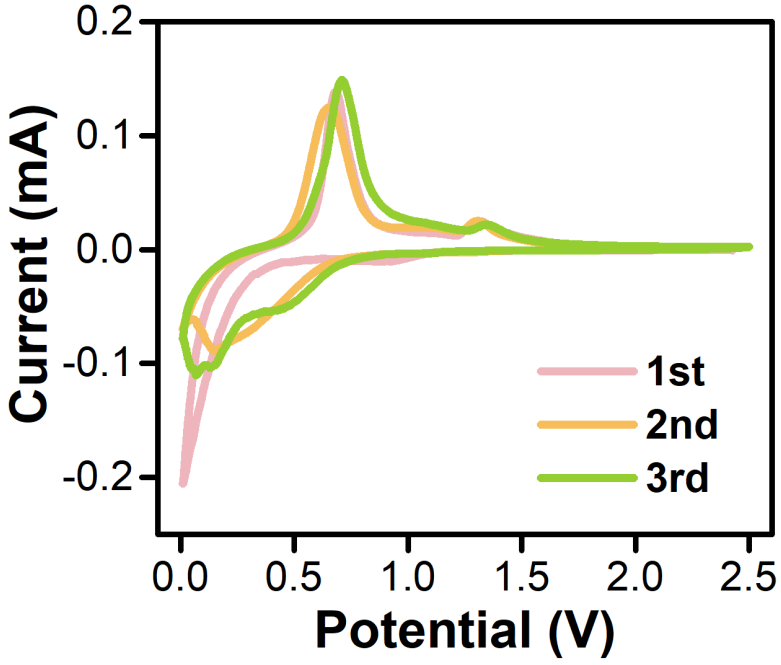

Figure S9. The first three CV curves of Sb anode with a scanning rate of 0.05 mV s^{-1}.

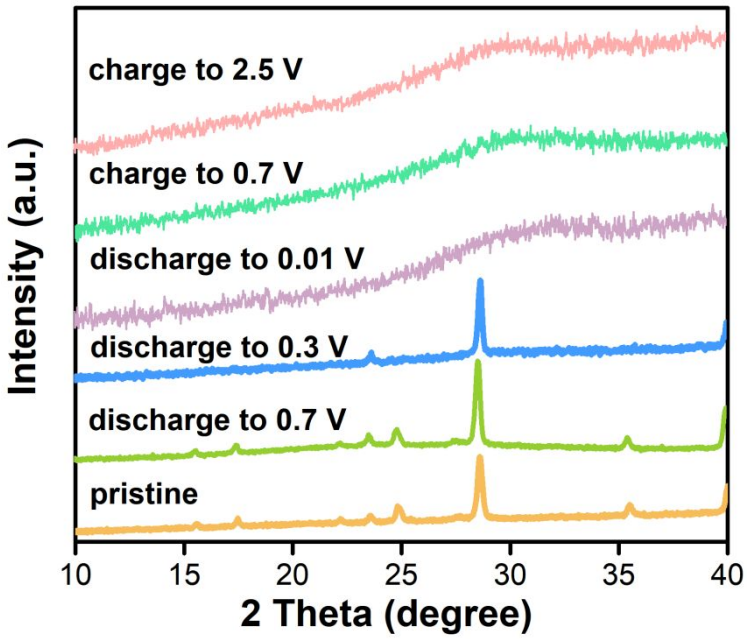

Figure S10. XRD patterns of Sb/Sb_2S_3@CHT anode at different charge/discharge states.

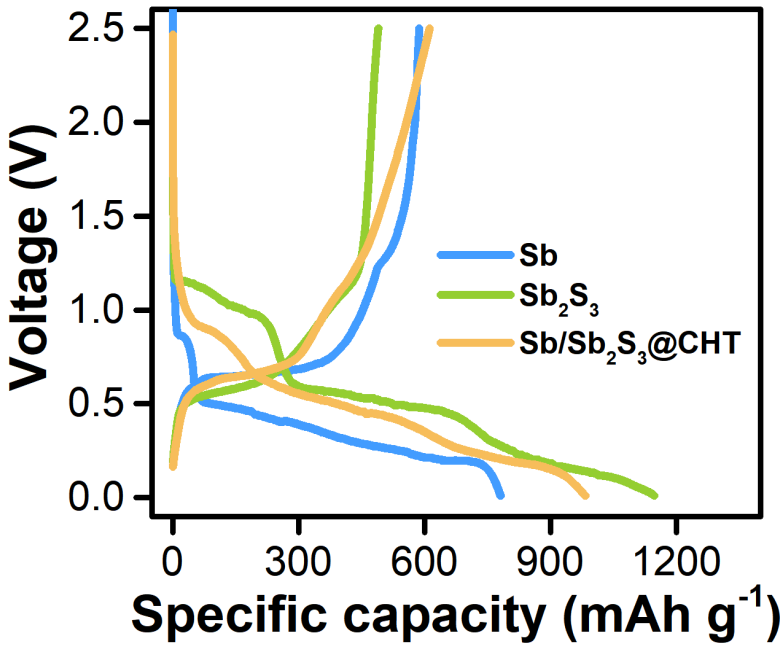

Figure S11. The first GCD curves of commercial Sb powders, as-prepared Sb_2S_3 nanorods and Sb/Sb_2S_3@CHT.

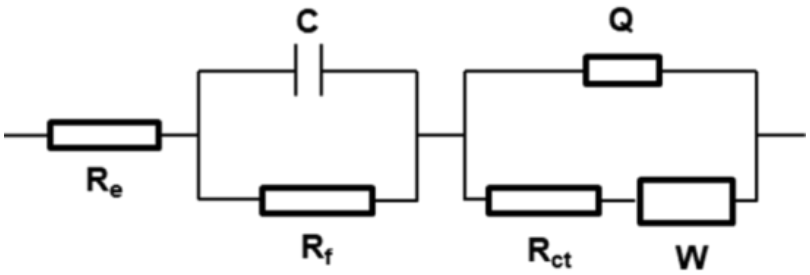

Figure S12. Equivalent circuit model used to fit EIS. R_e presents the ohmic resistance of electrode; C and R_f are the capacitance and the SEI impedance; W presents the Warburg impedance; R_{ct} stand for charge transfer resistance; Q is associated with the the double layer capacitance and passivation film.[1]

Table S1. The values of R_{ct} and R_f obtained by circuit simulation based on ex-situ EIS.

Discharge voltage (V)	**2.68**	**1**	**0.8**	**0.6**	**0.5**	**0.4**	**0.3**	**0.2**	**0.1**	**0.01**
R_{ct} (Ω)	10300	8200	3800	3125	3348	3329	3109	3067	3517	3405
R_f(Ω)	129800	9337	11730	764.4	4.189	4.891	5.505	5.624	5.608	5.865
Charge voltage (V)	**0.5**	**0.6**	**0.7**	**0.8**	**1.0**	**1.2**	**1.4**	**1.8**	**2.0**	**2.5**
R_{ct} (Ω)	3773	3223	1933	2101	2032	1950	2114	1913	1906	1676
R_f(Ω)	5.17	5.745	10.9	12.65	12.91	13.13	13.43	12.24	12.04	14.64

Table S2. Comparison of Sb/Sb_2S_3@CHT anode with other Sb-based materials in terms of rate and cycle performances.

Materials [Ref]	Rate performance	Cycle stability
Sb/Sb_2S_3@CHT (This work)	608.9 mAh g^{-1} at 50 mA g^{-1} 173.2 mAh g^{-1} at 2000 mA g^{-1}	400.9 mA h g^{-1} at 200 mA g^{-1} after 200 cycles; 147.5 mA h g^{-1} at 1000 mA g^{-1} after 3500 cycles
Sb@CN nanofibers [2]	324.72 mAh g^{-1} at 300 mA g^{-1} 243.58 mAh g^{-1} at 500 mA g^{-1}	212.7 mAh g^{-1} at 5 A g^{-1} after 1000 cycles
SnSb [3]		282 mAh g^{-1} at C/5 after 40 cycles
Sb-Co [4]		402.7 mAh g^{-1} at 60 mA g^{-1} after 100 cycles
Sb-NPs@PC [5]	551 mAh g^{-1} at 50 mA g^{-1} 160 mAh g^{-1} at 2000 mA g^{-1}	497 mAh g^{-1} at 100 mA g^{-1} over 100 cycles
Sb@RGO [6]	381 mAh g^{-1} at 100 mA g^{-1}; 222 mAh g^{-1} at 1000 mA g^{-1}	210 mA h g^{-1} at 500 mA g^{-1} for 200 cycles
Sb/Na−Ti_3C_2T [7]	127.0 mAh g^{-1} at 2.0 A g^{-1}	258 mAh g^{-1} at 0.5 A g^{-1} after 1200 cycles
Sb@CNFs [8]	448 mAh g^{-1} at 100 mA g^{-1}; 121 mAh g^{-1} at 2000 mA g^{-1}	338 mA h g^{-1} at 200 mA g^{-1} after 200 cycles; 227 mA h g^{-1} at 1000 mA g^{-1} after 1000 cycles
Sb_2Se_3@C microtube [9]	500.4 mAh g^{-1} at 50 mA g^{-1} 173.8 mAh g^{-1} at 2000 mA g^{-1}	191.4 mAh g^{-1} at 500 mA g^{-1} after 400 cycles
Sb_2Se_3@ NC@rGO [10]	595 mAh g^{-1} at 50 mA g^{-1} 130 mAh g^{-1} at 1000 mA g^{-1}	250 mAh g^{-1} at 500 mA g^{-1} after 350 cycles
Sb_2O_3-RGO [11]	326 mA h g^{-1} at 100 mA g^{-1} 172 mA h g^{-1} at 1000 mA g^{-1}	309 mAh g^{-1} at 100 mA g^{-1} after 100 cycles; 201 mAh g^{-1} at 500 mA g^{-1} after 3300 cycles
Sb_2S_3@C [12]	548 mA h g^{-1} at 50 mA g^{-1} 163 mA h g^{-1} at 1000 mA g^{-1}	293 mAh g^{-1} at 50 mA g^{-1} after 50 cycles
Sb/CNS [13]	395.5 mA h g^{-1} at 50 mA g^{-1} 101.4 mA h g^{-1} at 2000 mA g^{-1}	247 mAh g^{-1} at 200 mA g^{-1} after 600 cycles

Sb_2S_3–rGO [14]	509 mA h g^{-1} at 100 mA g^{-1} 286 mA h g^{-1} at 1000 mA g^{-1}	110 mAh g^{-1} at 50 mA g^{-1} after 50 cycles
Sn-Sb [15]	479 mA h g^{-1} at 100 mA g^{-1} 118 mA h g^{-1} at 5000 mA g^{-1}	296 mAh g^{-1} at 500 mA g^{-1} after 150 cycles
Sb−C−rGO [16]	388 mA h g^{-1} at 200 mA g^{-1} 195 mA h g^{-1} at 1500 mA g^{-1}	245 mAh g^{-1} at 500 mA g^{-1} after 100 cycles
Sb-P-C [17]		402 mAh g^{-1} at 50 mA g^{-1} after 50 cycles
Sb/RGO [18]		250 mAh g^{-1} after 100 cycles
SnSb-G-C [19]	207.27 mAh g^{-1} at 1000 mA g^{-1}	275.14 mAh g^{-1} at 100 mA g^{-1} after 100 cycles
Sb-G-C [20]	120.83 mAh g^{-1} at 1000 mA g^{-1}	204 mAh g^{-1} at 100 mA g^{-1} after 100 cycles
Sb@G@C [21]	127 mA h g^{-1} at 2000 mA g^{-1}	160 mAh g^{-1} at 1000 mA g^{-1} after 800 cycles

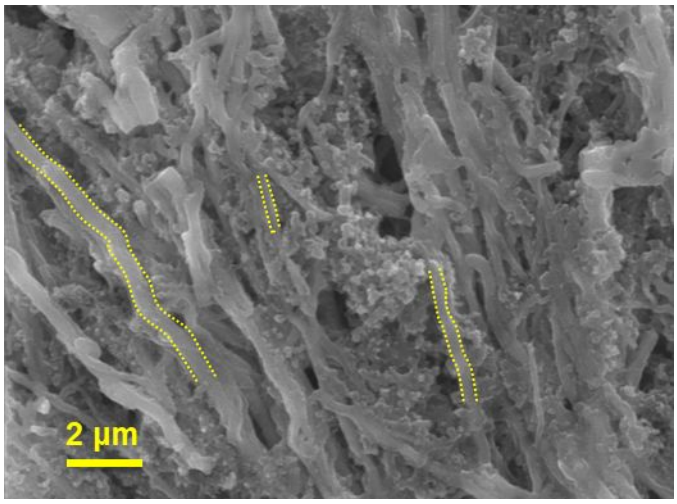

Figure S13. SEM image of Sb/Sb_2S_3@CHT anode after rate test.

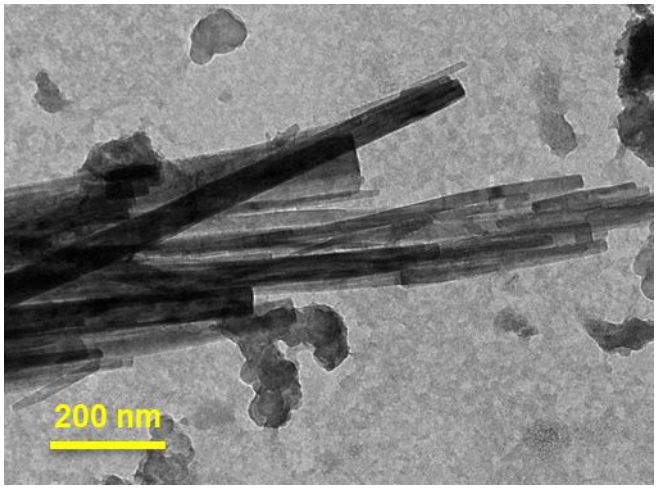

Figure S14. TEM image of Sb/Sb_2S_3@CHT after rate test.

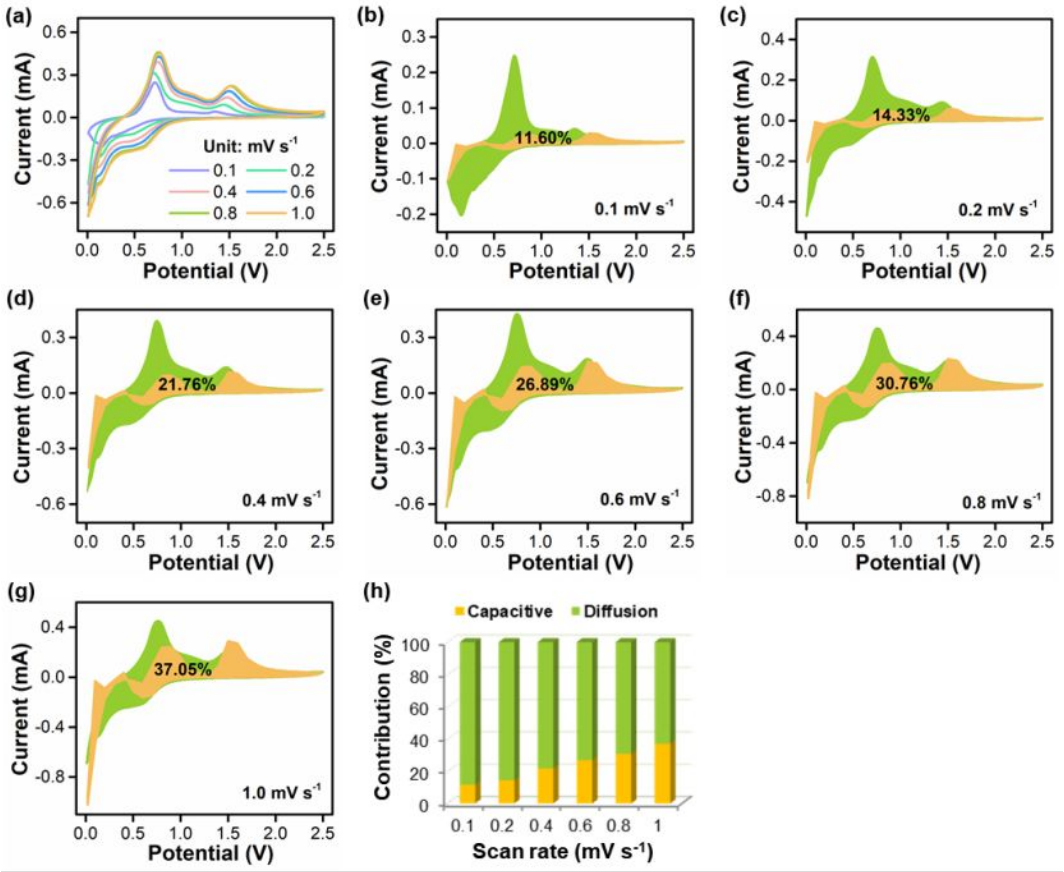

Figure S15. (a) CV curves of Sb anode scanned at various rates. (b-g) Capacitance contribution of Sb anode scanned at various rates. (h) Comparison of capacitance-controlled and diffusion-controlled contribution of Sb anode at various scanning rates.

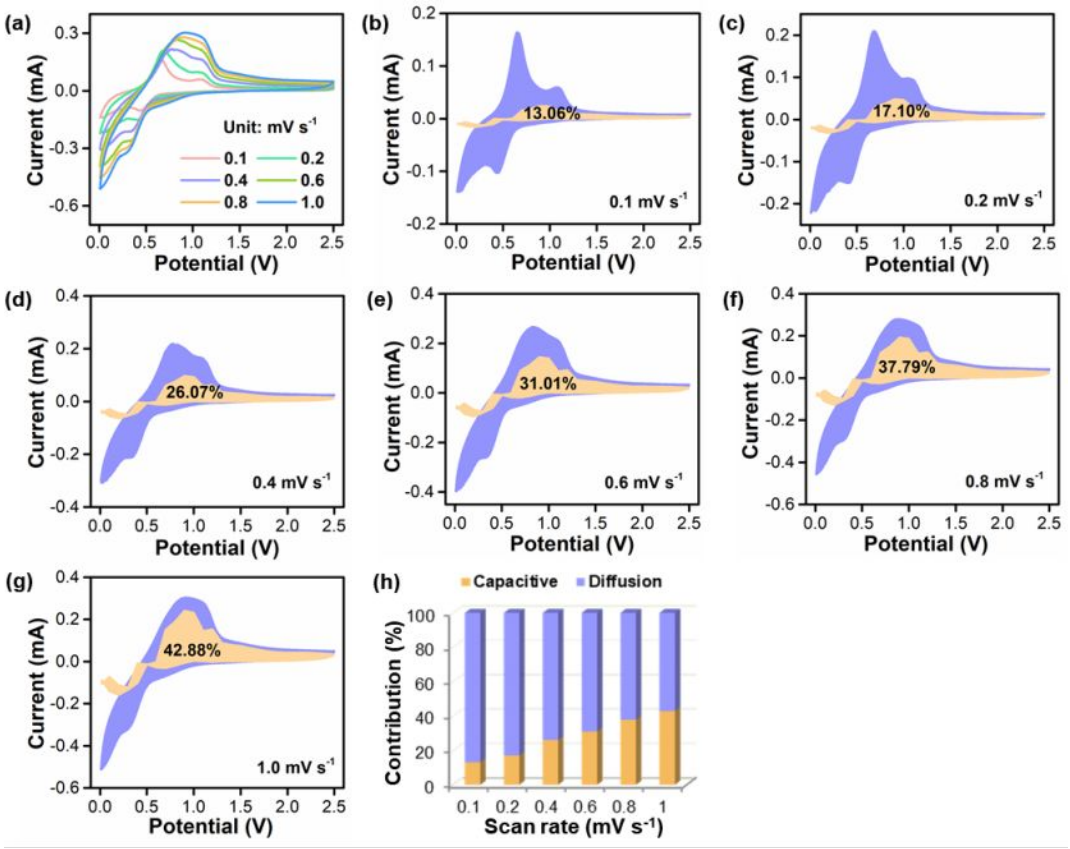

Figure S4. (a) CV curves of Sb_2S_3 anode scanned at various rates. (b-g) Capacitance contribution of Sb_2S_3 anode scanned at various rates. (h) Comparison of capacitance-controlled and diffusion-controlled contribution of Sb_2S_3 anode at various scanning rates.

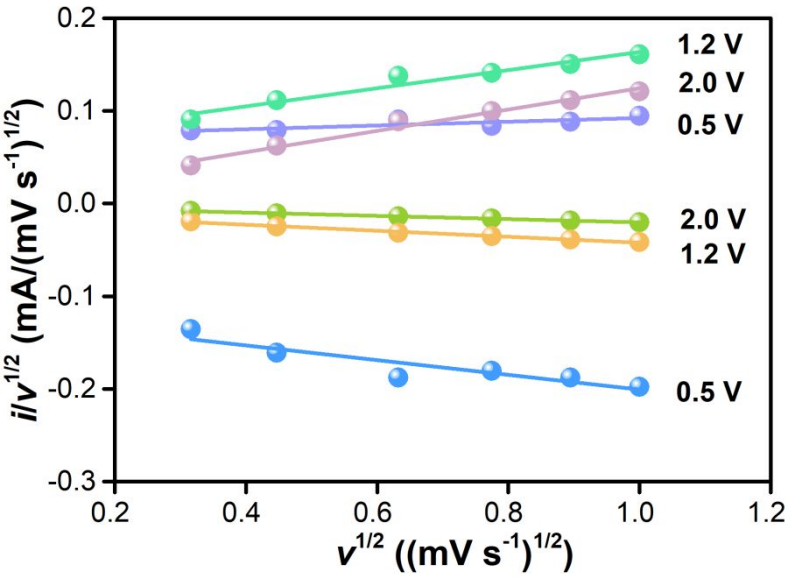

Figure S17. The relationship between $i/v^{1/2}$ and $v^{1/2}$.

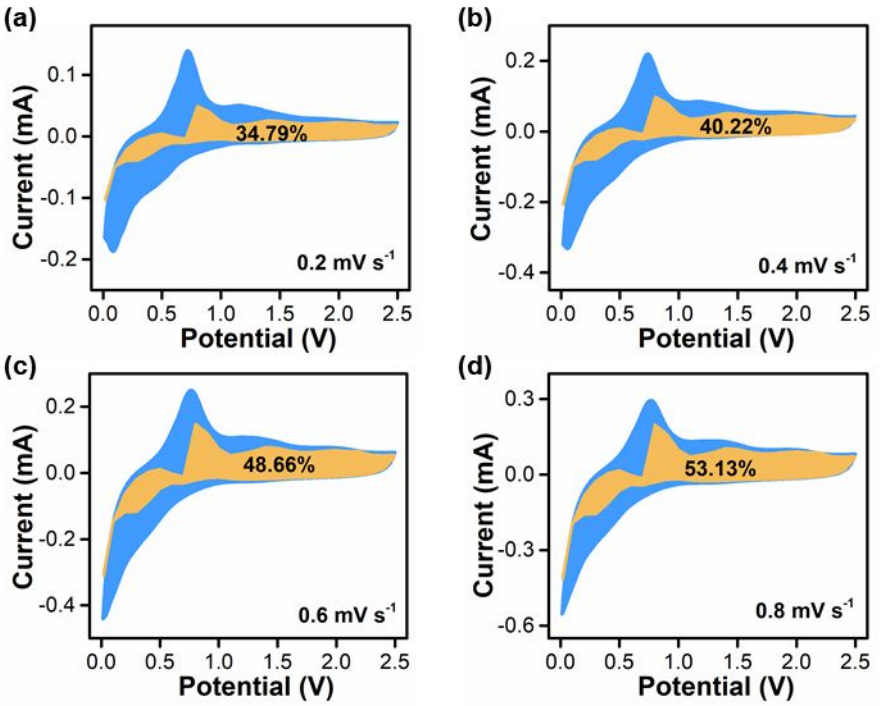

Figure S18. Capacitance contribution of Sb/Sb_2S_3@CHT anode scanned at 0.2 mV s^{-1} (a), 0.4 mV s^{-1} (b), 0.6 mV s^{-1} (c) and 0.8 mV s^{-1} (d), respectively.

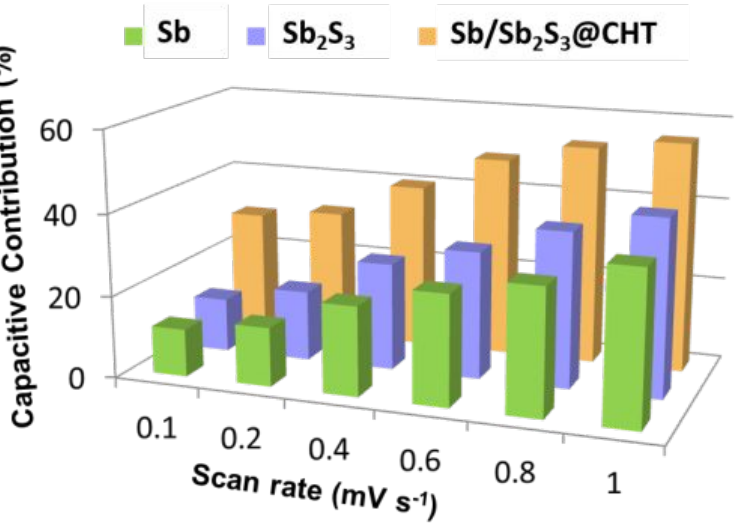

Figure S19. The comparison of capacitive contribution of Sb, Sb_2S_3 and Sb/Sb_2S_3@CHT half-cells at different scan rate.

Table S3. The values of R_{ct} obtained by circuit simulation based on the EIS before and after cycles.

Cycle number	0	20	60	100	140	180	220	260	300
R_{ct} (Ω)	10300	1621	1077	553.1	527.1	350.3	513.1	476	405.8
R_f(Ω)	558500	6.87	2.49	15	14	8.38	9.63	9.08	9

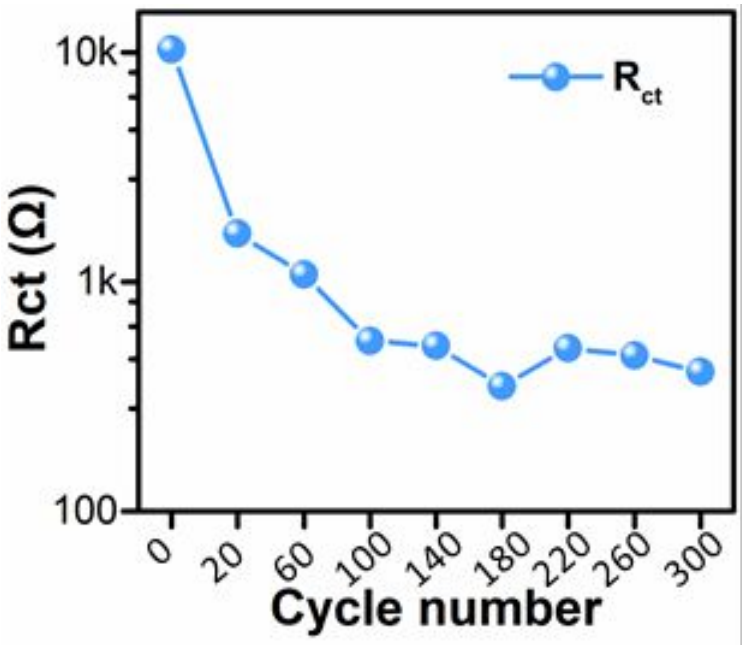

Figure S20. The R_{ct} change of Sb/Sb_2S_3@CHT anode before and after cycles.

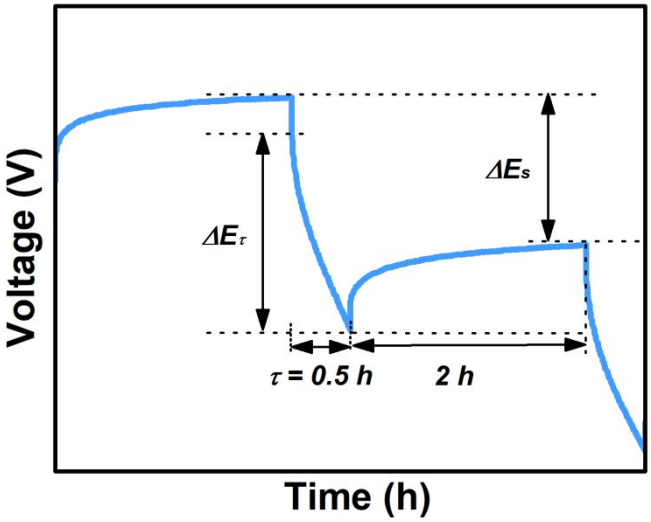

Figure S21. Schematic diagram of parameter determination of galvanostatic intermittent titration.

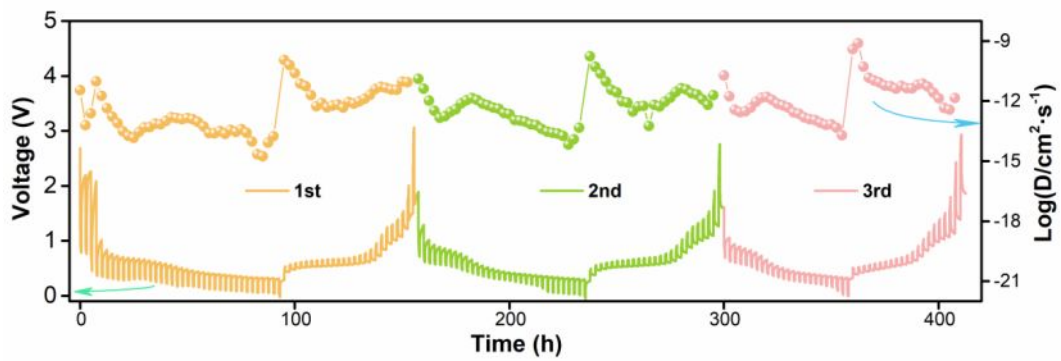

Figure S22. GITT curves and calculated K^+ diffusion coefficient of Sb anode tested at the first three cycles.

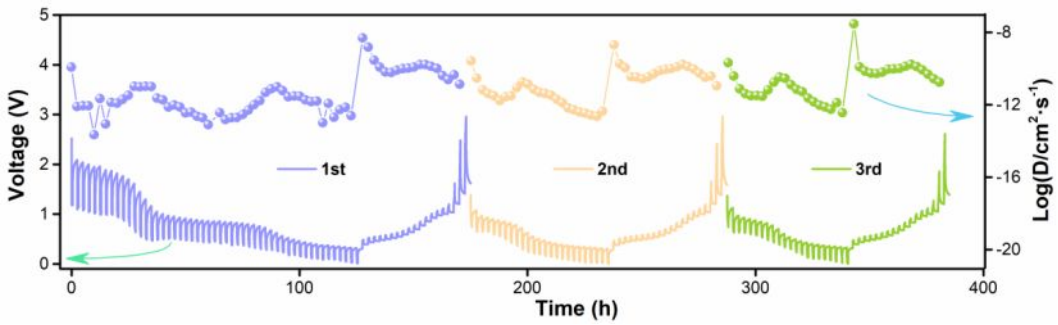

Figure S23. GITT curves and calculated K^+ diffusion coefficient of Sb_2S_3 anode tested at the first three cycles.

Table S4. Averge K^+ diffusion coefficients during different charge/discharge process.

Averge Log(D/cm^2·s^{-1})	1 st (discharge)	1 st (charge)	2 nd (discharge)	2 nd (charge)	3 rd (discharge)	3 rd (charge)
Sb/Sb_2S_3@CHT	-11.1715	-9.38319	-10.7128	-9.45759	-10.6369	-9.47826
Sb_2S_3	-11.9805	-9.92718	-11.5657	-10.1344	-11.3179	-9.97929
Sb	-13.1349	-11.5462	-12.716	-11.7051	-12.48	-11.1642

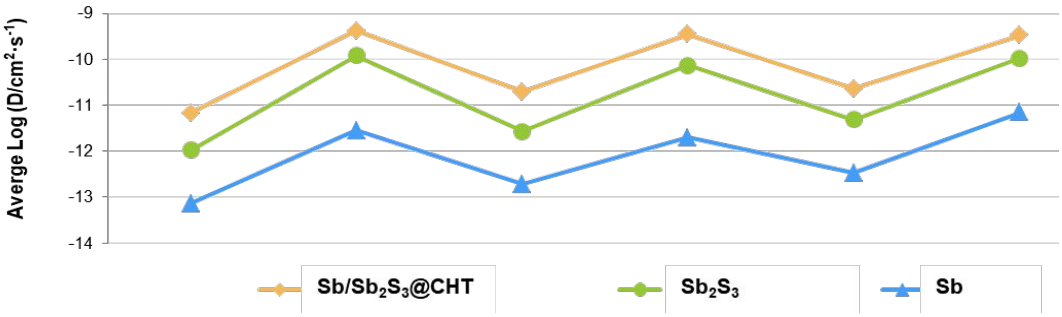

Figure S24. Comparison of averge K^+ diffusion coefficients of Sb, Sb_2S_3 and Sb/Sb_2S_3@CHT anodes.

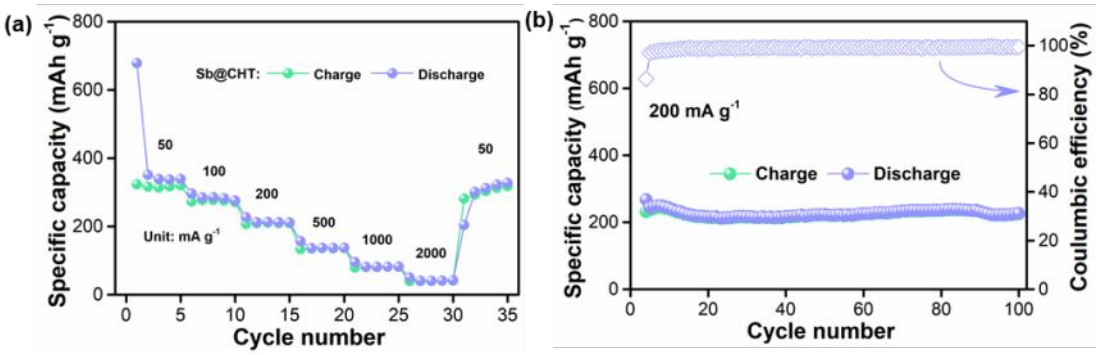

Figure S25. (a) Rate performance of Sb@CHT. (b) Cycle performance of Sb@CHT at 200 mA g^{-1}.

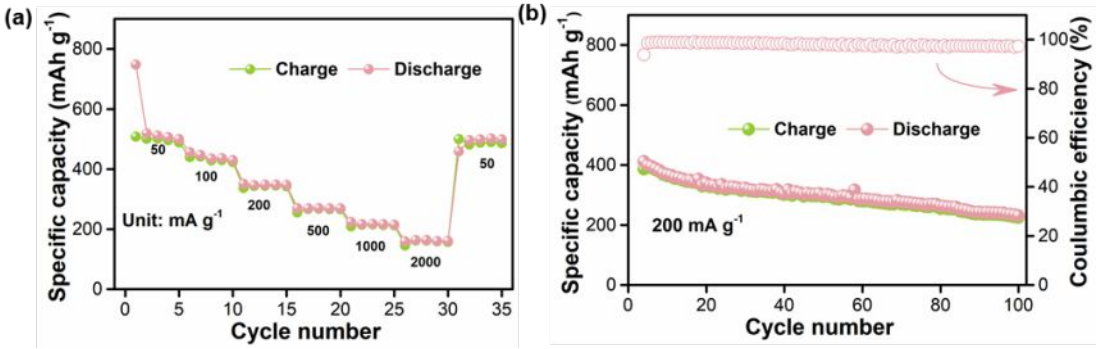

Figure S26. (a) Rate performance of Sb/Sb_2S_3@CHT with 1 M KFSI in EC/DEC as electrolyte. (b) Cycle performance of Sb/Sb_2S_3@CHT at 200 mA g^{-1} with 1 M KFSI in EC/DEC as electrolyte.

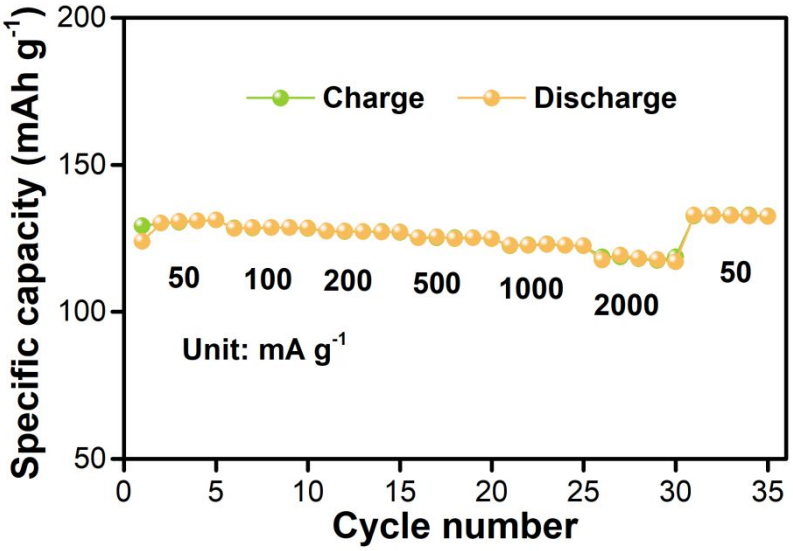

Figure S27. Rate performance of A-PTCDA.

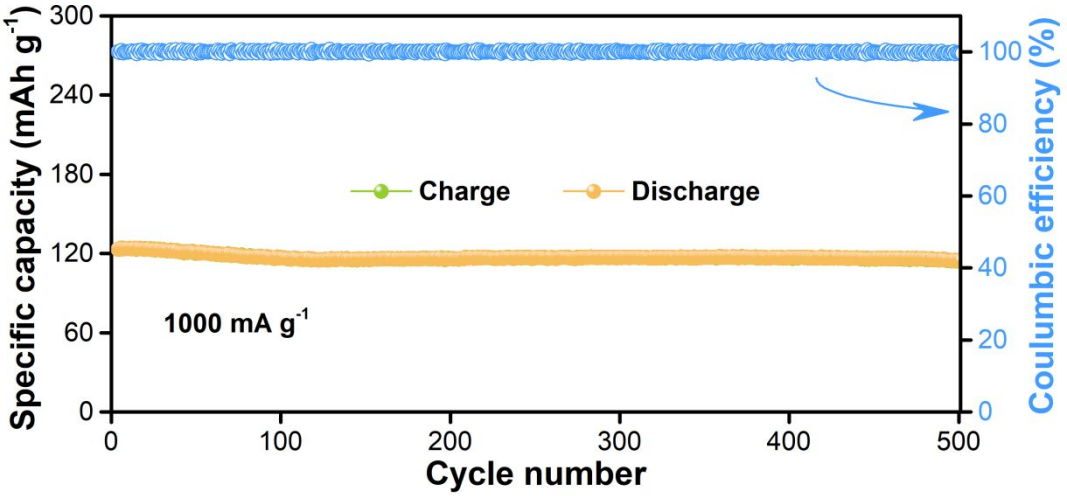

Figure S28. Cycle performance of A-PTCDA at 1000 mA g^{-1}.

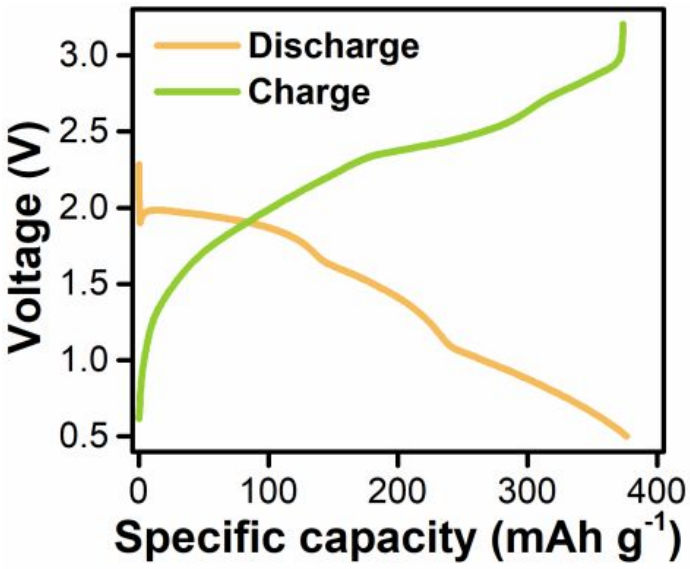

Figure S29. The first cycle discharge and charge curves of Sb/Sb_2S_3@CHT//A-PTCDA device.

Ⅱ. Reference

(1) Jian, X. M.; Wenren, H. Q.; Huang, S.; Shi, S. J.; Wang, X. L.; Gu, C. D.; Tu, J. P., Oxalic Acid-Assisted Combustion Synthesized $LiVO_3$ Cathode Material for Lithium Ion Batteries. *J. Power Sources* **2014**, *246*, 417-422.

(2) Liu, D.; Yang, L.; Chen, Z.; Zou, G.; Hou, H.; Hu, J.; Ji, X., Ultra-Stable Sb Confined into N-Doped Carbon Fibers Anodes for High-Performance Potassium-Ion Batteries. *Sci. Bull.* **2020**, *65*, 1003-1012.

(3) Gabaudan, V.; Berthelot, R.; Sougrati, M. T.; Lippens, P.-E.; Monconduit, L.; Stievano, L., SnSb vs. Sn: Improving the Pperformance of Sn-Based Anodes for K-Ion Batteries by Synergetic Alloying with Sb. *J. Mater. Chem. A.* **2019**, *7*, 15262-15270.

(4) Zhang, Y.; Li, M.; Huang, F.; Li, Y.; Xu, Y.; Wang, F.; Yao, Q.; Zhou, H.; Deng, J., 3D Porous Sb-Co Nanocomposites as Advanced Anodes for Sodium-Ion Batteries and Potassium-Ion Batteries. *Appl. Surf. Sci.* **2020**, *499*, 143907.

(5) Cheng, N.; Zhao, J.; Fan, L.; Liu, Z.; Chen, S.; Ding, H.; Yu, X.; Liu, Z.; Lu, B., Sb-MOFs Derived Sb Nanoparticles@Porous Carbon for High Performance Potassium-Ion Batteries Anode. *Chem. Commun.* **2019**, *55*, 12511-12514.

(6) Yi, Z.; Lin, N.; Zhang, W.; Wang, W.; Zhu, Y.; Qian, Y., Preparation of Sb Nanoparticles in Molten salt and Their Potassium Storage Performance and Mechanism. *Nanoscale* **2018**, *10*, 13236-13241.

(7) Zhao, R.; Di, H.; Wang, C.; Hui, X.; Zhao, D.; Wang, R.; Zhang, L.; Yin, L., Correction to Encapsulating Ultrafine Sb Nanoparticles in Na^+ Pre-Intercalated 3D

Porous $Ti_3C_2T_x$ MXene Nanostructures for Enhanced Potassium Storage Performance. *ACS Nano* **2021**, *15*, 5773-5773.

(8) Huang, H.; Wang, J.; Yang, X.; Hu, R.; Liu, J.; Zhang, L.; Zhu, M., Unveiling the Advances of Nanostructure Design for Alloy-Type Potassium-Ion Battery Anodes via In Situ TEM. *Angew. Chem. Int. Ed.* **2020**, *59*, 14504-14510.

(9) Yi, Z.; Qian, Y.; Tian, J.; Shen, K.; Lin, N.; Qian, Y., Self-Templating Growth of Sb_2Se_3@C Microtube: A Convention-Alloying-Type Anode Material for Enhanced K-Ion Batteries. *J. Mater. Chem. A* **2019**, *7*, 12283-12291.

(10) Wang, S.; Xiong, P.; Guo, X.; Zhang, J.; Gao, X.; Zhang, F.; Tang, X.; Notten, P. H. L.; Wang, G., A Stable Conversion and Alloying Anode for Potassium-Ion Batteries: A Combined Strategy of Encapsulation and Confinement. *Adv. Funct. Mater*. **2020**, *30*, 2001588.

(11) Li, J.; Zhuang, N.; Xie, J.; Li, X.; Zhuo, W.; Wang, H.; Na, J. B.; Li, X.; Yamauchi, Y.; Mai, W., K-Ion Storage Enhancement in Sb_2O_3/Reduced Graphene Oxide Using Ether-Based Electrolyte. *Adv. Energy Mater.* **2020**, *10*, 1903455.

(12) Cheng, Y.; Yao, Z.; Zhang, Q.; Chen, J.; Ye, W.; Zhou, S.; Liu, H.; Wang, M.-S., In Situ Atomic-Scale Observation of Reversible Potassium Storage in Sb_2S_3@Carbon Nanowire Anodes. *Adv. Funct. Mater.* **2020**, *30*, 2005417.

(13) Han, Y.; Li, T.; Li, Y.; Tian, J.; Yi, Z.; Lin, N.; Qian, Y., Stabilizing Antimony Nanocrystals within Ultrathin Carbon Nanosheets for High-Performance K-Ion Storage. *Energy Storage Mater.* **2019**, *20*, 46-54.

(14) Lakshmi, V.; Mikhaylov, A. A.; Medvedev, A. G.; Zhang, C.; Ramireddy, T.;

Rahman, M. M.; Cizek, P.; Golberg, D.; Chen, Y.; Lev, O.; Prikhodchenko, P. V.; Glushenkov, A. M., Probing Electrochemical Reactivity in an Sb_2S_3-Containing Potassium-Ion Battery Anode: Observation of an Increased Capacity. *J. Mater. Chem. A* **2020**, *8*, 11424-11434.

(15) Ding, H.; Wang, J.; Fan, L.; Liu, Z.; Jia, X.; Yu, X.; Lu, B., Sn-Sb Compounds with Novel Structure for Stable Potassium Storage. *Chem. Eng. J.* **2020**, *395*, 125147.

(16) Ko, Y. N.; Choi, S. H.; Kim, H.; Kim, H. J., One-Pot Formation of Sb–Carbon Microspheres with Graphene Sheets: Potassium-Ion Storage Properties and Discharge Mechanisms. *ACS Appl. Mater. Interfaces* **2019**, *11*, 27973-27981.

(17) Sultana, I.; Rahman, M. M.; Liu, J.; Sharma, N.; Ellis, A. V.; Chen, Y.; Glushenkov, A. M., Antimony-Carbon Nanocomposites for Potassium-Ion Batteries: Insight into the Failure Mechanism in Electrodes and Possible Avenues to Improve Cyclic Stability. *J. Power Sources* **2019**, *413*, 476-484.

(18) Wang, L.; Jia, J.; Wu, Y.; Niu, K., Antimony/Reduced Graphene Oxide Composites as Advanced Anodes for Potassium Ion Batteries. *J. Appl. Electrochem.* **2018**, *48*, 1115-1120.

(19) Huang, Z.; Chen, Z.; Ding, S.; Chen, C.; Zhang, M., Multi-Protection from Nanochannels and Graphene of SnSb-Graphene-Carbon Composites Ensuring High Properties for Potassium-Ion Batteries. *Solid State Ionics* **2018**, *324*, 267-275.

(20) Huang, Z.; Ding, S.; Li, P.; Chen, C.; Zhang, M., Flexible Sb-Graphene-Carbon Nanofibers as Binder-Free Anodes for Potassium-Ion Batteries with Enhanced Properties. *Nanotechnology* **2020**, *32*, 025401.

(21) Liu, Q.; Fan, L.; Ma, R.; Chen, S.; Yu, X.; Yang, H.; Xie, Y.; Han, X.; Lu, B., Super Long-Life Potassium-Ion Batteries Based on an Antimony@Carbon Composite Anode. *Chem. Commun.* **2018**, *54*, 11773-11776.